The Role of Thermomechanical Routes on the Distribution of Grain Boundary and Interface Plane Orientations in Transformed Microstructures

HOSSEIN BELADI and GREGORY S. ROHRER

In the current study, a series of thermomechanical routes were used to produce different microstructures (*i.e.*, ferrite and martensite) in low-carbon low alloy steels. The five-parameter grain boundary character distribution was measured for all microstructures. The thermomechanical processing route altered the texture of the fully ferritic microstructure and significantly influenced the anisotropy of the grain boundary character distribution. Generally, the population of (111) planes increased with an increase in the γ-fiber texture for the ferritic microstructure, but it did not change the shape of the grain boundary plane distribution at specific misorientations. The most commonly observed boundaries in the fully ferritic structures produced through different routes were {112} symmetric tilt boundaries with the $\Sigma 3 = 60$ deg/[111] misorientation; this boundary also had a low energy. However, the grain boundary plane distribution was significantly changed by the phase transformation path (*i.e.*, ferrite *vs* martensite) for a given misorientation. In the martensitic steel, the most populous $\Sigma 3$ boundary was the {110} symmetric tilt boundary. This results from the crystallographic constraints associated with the shear transformation (*i.e.*, martensite) rather than the low-energy interface that dominates in the diffusional phase transformation (*i.e.*, ferrite).

DOI: 10.1007/s11661-016-3630-4

I. INTRODUCTION

THERE is an ongoing requirement for material and product innovations to meet the increasing demand of higher performance at minimal cost. The development of these materials requires a deep understanding about the influence of each microstructure constituent, and their interactions, on the property of interest. An important active structural element is the grain boundary whose characteristics control a number of the properties of polycrystalline materials. The manipulation of grain boundary structure is one of the fundamental goals of the materials science and engineering field since the mid-1980s.[1] The main challenge is to control the population and connectivity of certain grain boundary types relevant to the property of interest to enhance material performance.

The typical approach is iterative thermomechanical processing (*e.g.*, recrystallization) where the nucleation and growth of grains are controlled to a large extent by low-energy boundary network configurations.[2] Many technologically important metals such as steel and titanium alloys do not, however, maintain the high-temperature microstructure and undergo phase transformation on cooling. Because the resultant microstructure depends on the phase transformation path, this is the most effective way to tailor the microstructure and properties. For instance, for a given steel composition, the austenite state (grain size and density of various defects) and cooling rate are the most important thermomechanical parameters for the control of the different phases at room temperature (*e.g.*, polygonal ferrite, bainite or martensite). The transformation of austenite to ferrite takes place at a relatively high temperature (during slow cooling) where both nucleation and growth processes are controlled by the diffusion/reconstructive mechanism. Alternatively, the displacive shear mechanism occurs during the austenite to martensite phase transformation on rapid cooling. Bainite is usually formed at an intermediate temperature range between those of the reconstructive (ferrite) and displacive (martensite) phases. It was recently found that the grain boundary network is largely controlled by the phase transformation mechanism constraints rather than the relative energies of the interfaces.[3,4] The purpose of this paper is to review and compare the grain boundary character distributions of four microstructures processed in different ways. These distributions have been previously reported in different contexts,[3,5,6] but here we focus on the role of the transformation path on the grain boundary character distribution.

HOSSEIN BELADI, Senior Research Academic, is with the Institute for Frontier Materials, Deakin University, Geelong, VIC 3216, Australia. Contact e-mail: hossein.beladi@deakin.edu.au GREGORY S. ROHRER, W.W. Mullins Professor and Head, is with the Department of Materials Science and Engineering, Carnegie Mellon University, Pittsburgh, PA 15213-3890.

Manuscript submitted March 28, 2016.
Article published online July 5, 2016

II. EXPERIMENTAL PROCEDURE

Thermomechanical processing is the main approach used to manipulate the final microstructures of steels. Deformation can be applied at different temperature regimes depending on the steel composition and the desired final microstructure. Here, two steel compositions were used to study the influence of thermomechanical processing routes on the grain boundary characteristics formed through different phase transformation paths in steel (Table I). Figure 1 schematically illustrates the different thermomechanical routes used for these steels. Details of the thermomechanical routes and employed apparatus can be found in the relevant references cited in Table II.

Steel A was subjected to different thermomechanical routes that lead to polygonal ferrite microstructures with different overall crystallographic textures or to a fully martensitic structure, depending on the cooling. First, the steel was reheated to 1473 K (1200 °C) and then deformed to a strain of 0.5 followed by holding for 60 s to obtain a fully recrystallized austenite microstructure. Afterward, the samples were subjected to two different post-deformation routes: (i) immediately water-quenched to form the fully martensitic microstructure (*i.e.*, route A, Figure 2(a), or (ii) cooled to 923 K (650 °C) at 10 K/s and held for 6000 s to fully transform the steel to ferrite with an average grain size of 35 μm (*i.e.*, route B, Figure 2(b)).

The hot deformation of austenite mostly leads to the restoration processes (*i.e.*, recovery/recrystallization, *e.g.*, route B). However, the addition of microalloying elements (*e.g.*, Nb, Mo) significantly retards the recrystallization below a certain temperature, the so-called nonrecrystallization temperature (*i.e.*, Tnr), through solute drag[7,8] and/or precipitation pinning[7] effects. This remarkably alters the extent of nucleation and the growth rate of transformed phases (*e.g.*, ferrite) through three mechanisms. First, it roughens the austenite grain boundary, enhancing ferrite nucleation sites. Second, the deformation induces intergranular defects, which are suitable for the nucleation of the transformed phase. Finally, it has a geometrical effect through pancaking the austenite grains, limiting the ferrite growth. Therefore, the deformation of austenite below Tnr leads to ferrite grain refinement. In another thermomechanical route, Steel A was, therefore, deformed at 1163 K (890 °C, below Tnr) to a strain of 1 after reheating at 1473 K (1200 °C). The sample was then cooled to 923 K (650 °C) and held for 600 s, resulting in a fully ferritic microstructure with an average grain size of ~6 μm (*i.e.*, route C, Figure 2(c)).

Table I. The Steel Compositions Used in the Current Study (in Weight Percent)

Steel	C	Mn	Si	Mo	Ti	Al	N
A	0.04	1.52	0.2	0.2	0.08	0.033	—
B	0.003	1.3	—	—	0.08	0.03	0.004

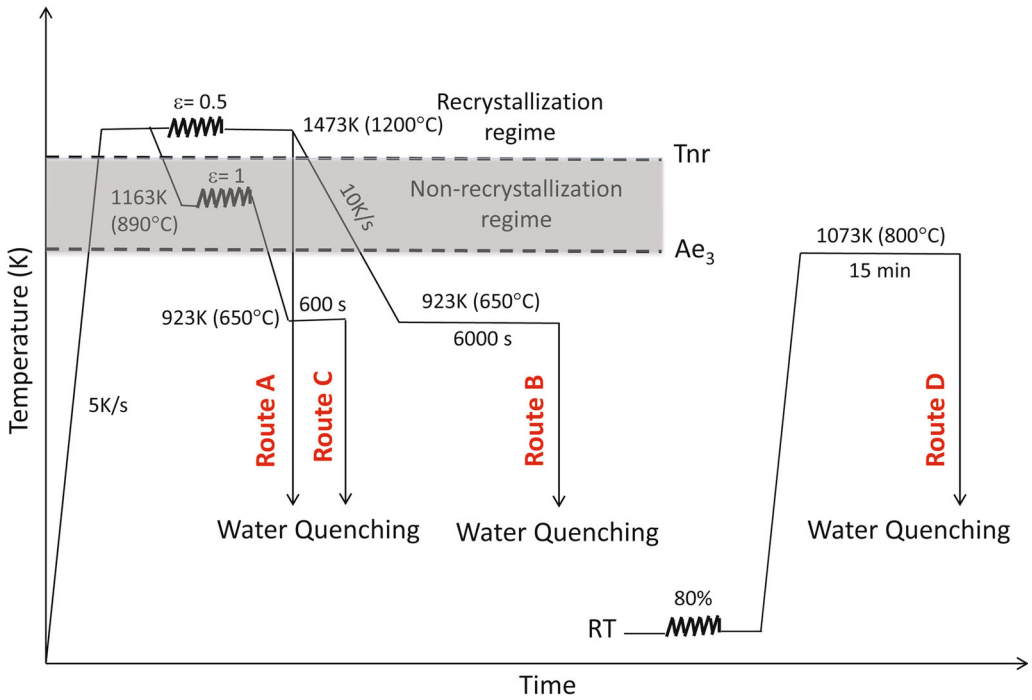

Fig. 1—Schematic representation of different thermomechanical routes. Tnr, Ae_3, and RT are non-recrystallization temperature, equilibrium austenite to ferrite transformation temperature, and room temperature, respectively.

Table II. The Details of EBSD Measurement for Different Microstructures

Thermomechanical Processing routes	Steel	Microstructure	Step Size (μm)	Area (μm^2)	Total Segments	References
Route A	A	martensite	0.15	85,000	93,400	3
Route B	A	ferrite	2	13,110,000	68,300	3
Route C	A	ferrite	0.2	255,000	178,400	5
Route D	B	ferrite	1	17,700,000	300,000	6

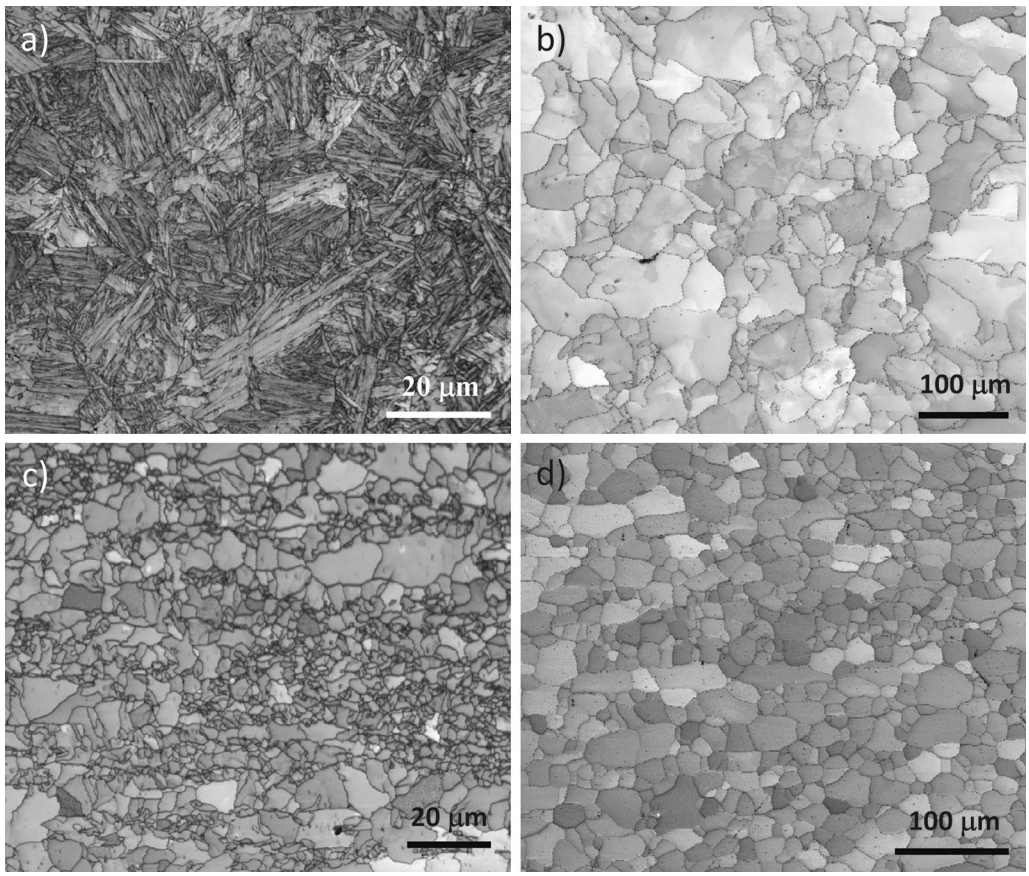

Fig. 2—The microstructures formed through different thermomechanical routes: (*a*) martensite, route A, (*b*) ferrite, route B, (*c*) ferrite, route C, and (*d*) ferrite, route D.

Steel B, which is an interstitial-free (IF) steel, was initially subjected to 80 pct cold-rolling reduction and then annealed at 1073 K (800 °C) for 15 minutes in a fluidized bed furnace under nitrogen gas. This resulted in a fully recrystallized ferrite microstructure with an average grain size of 13 μm (*i.e.*, route D, Figure 1(d)).

Electron Backscatter Diffraction (EBSD) was conducted to characterize the microstructures using a FEI Quanta SEM equipped with a focused ion beam. The details of EBSD measurement for each microstructure are summarized in Table II. Data acquisition and post-processing routines were performed using the TexSEM laboratories, Inc. software (TSL). To fully describe the crystallography of a grain boundary, five macroscopic parameters are required; three parameters to define the orientation relationship across the grain boundary (*i.e.*, the crystallographic lattice misorientation) and two parameters to specify the boundary plane orientation. Here, an automated stereological approach[9] was employed to measure the five crystallographic grain boundary parameters from extensive EBSD orientation maps collected for each microstructure.

A. *The Role of Thermomechanical Route on the Grain Boundary Character Distribution in Fully Ferritic Microstructures*

The microstructures resulting from the thermomechanical routes B, C, and D were fully ferritic and had equiaxed grain structures with different sizes. The misorientation angle distributions of the fully ferritic microstructures produced by different thermomechanical processing routes show obvious distinctions (Figure 3). The misorientation distribution of the fully ferritic microstructure transformed from the recrystallized austenite (*i.e.*, route B) has a significant peak above what is expected in a random distribution at about

60 deg (Figure 3(a)). The deformation of austenite below the Tnr temperature not only decreased the ferrite grain size, but also it altered the misorientation angle distribution (*i.e.*, route C). Here, the population of low-angle boundaries was somewhat increased at the expense of the 60 deg peak (Figure 3(b)). The population of low-angle boundaries was further enhanced when the ferritic structure of the IF steel was subjected to static recrystallization (*i.e.*, route D). Here, the misorientation angle distribution was relatively flat, displaying two small peaks at ~10 and 50 deg misorientation angles (Figure 3(c)). Knowledge of the crystallographic texture that results from these different processing routes can help to explain these differences.

For the thermomechanical processing routes B and C, the ferrite texture is governed by the parent austenite texture, which is strongly influenced by the steel composition[10] and thermomechanical routes.[11] The former can be ruled out here, as the same steel composition was used in both thermomechanical routes B and C. The recrystallization of austenite at high temperature [*i.e.*, above Tnr, 1473K (1200 °C)] leads to the formation of a predominant Cube texture (*i.e.*, $\{100\}\langle 001\rangle$).[12] During phase transformation, there is a crystallographic orientation relationship (OR) between the parent austenite and the daughter/product phase (*i.e.*, ferrite and martensite). The orientation relationship can vary from the Kurdjumov–Sachs (K–S) through the Nishiyama–Wasserman (N–W), which only differs by 5.26 deg.[13] Based on the orientation relationship between the parent austenite and products (*i.e.*, ferrite), the Cube texture is largely transformed into three main orientations consisted of Goss (*i.e.*, $\{110\}\langle 001\rangle$), rotated Cube (*i.e.*, $\{100\}\langle 011\rangle$), and the rotated Goss (*i.e.*, $\{110\}\langle 110\rangle$) during the phase transformation.[12] This is consistent with the overall texture observed in the fully ferritic structure transformed from the recrystallized austenite having a relatively weak texture with a maximum intensity of ~2.2 multiples of a random distribution, *i.e.*, MRD (Figure 4(a)).

Deformation below Tnr temperature retards recrystallization, resulting in the formation of multiple texture components in austenite, namely Copper $\{112\}\langle 111\rangle$, Brass $\{110\}\langle 112\rangle$, S $\{123\}\langle 634\rangle$, and Goss $\{110\}\langle 001\rangle$.[12] During the phase transformation, these components are transformed into several ferrite texture orientations such as transformed Brass (*i.e.*, $\{554\}\langle 225\rangle$ to $\{111\}\langle 112\rangle$), transformed Copper (*i.e.*, $\{112\}\langle 110\rangle$ to $\{113\}\langle 110\rangle$), and rotated Cube (*i.e.*, $\{100\}\langle 011\rangle$).[12] As a result, the overall ferrite texture strongly increased to ~3.9 MRD, revealing multiple peaks along the γ-fiber (*i.e.*, $\langle 111\rangle$// Normal direction, Figure 4(b)). The γ-fiber texture is significantly enhanced when the fully ferritic structure was subjected to the static recrystallization (*i.e.*, route D). Here, the typical γ-fiber texture was observed having a texture strength of ~12 MRD (Figure 4(c)). It has been

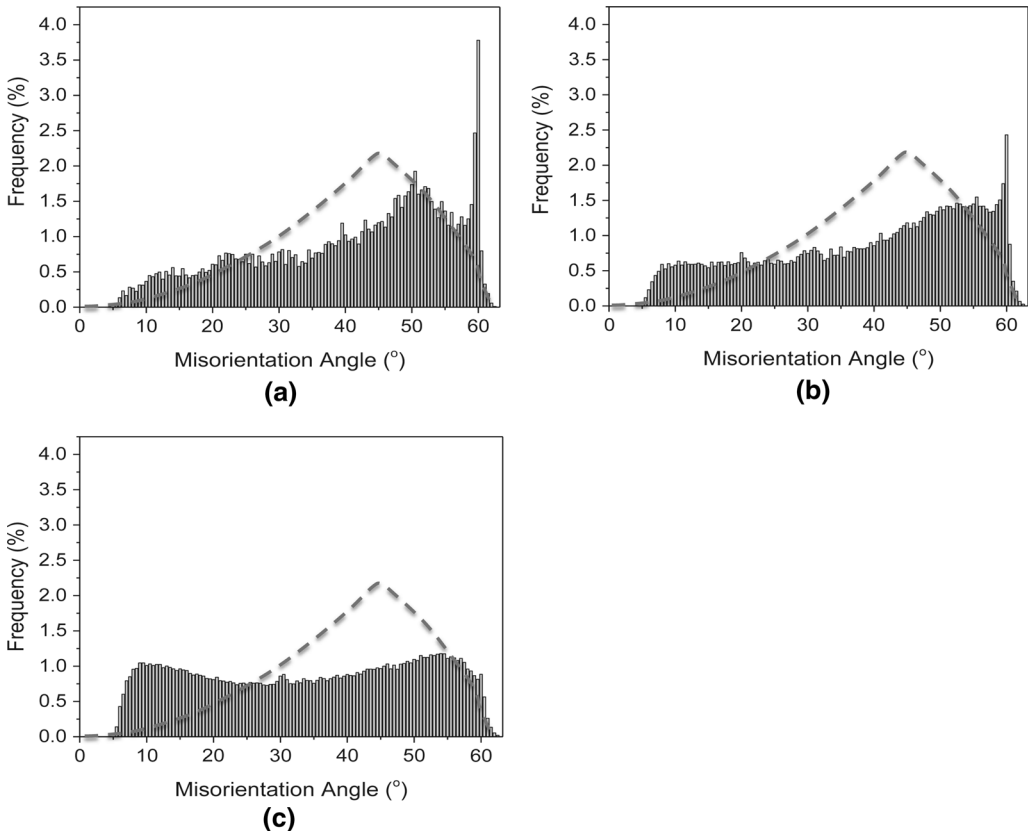

Fig. 3—Misorientation angle distribution for the ferritic microstructures formed through different thermomechanical routes: (*a*) route B, (*b*) route C, and (*c*) route D. The dash line curve represents the random misorientation angle distribution. (a), (b), and (c) are printed with permission from Refs. [3], [5], and [6], respectively.

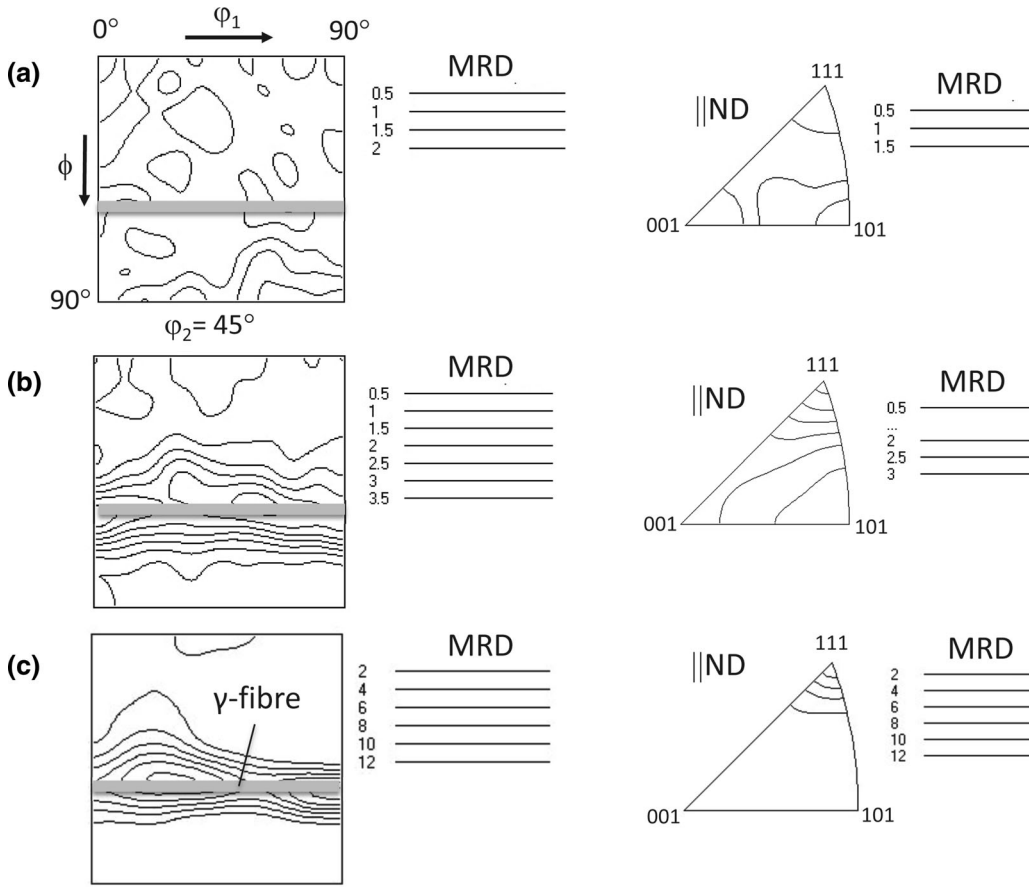

Fig. 4—Orientation distribution function of the ferritic microstructures produced through different thermomechanical routes and the corresponding inverse pole figures along the normal direction (ND). MRD is multiples of a random distribution. (*a*) route B, (*b*) route C, and (*c*) route D. (b) and (c) are printed with permission from Refs. [5] and [6], respectively.

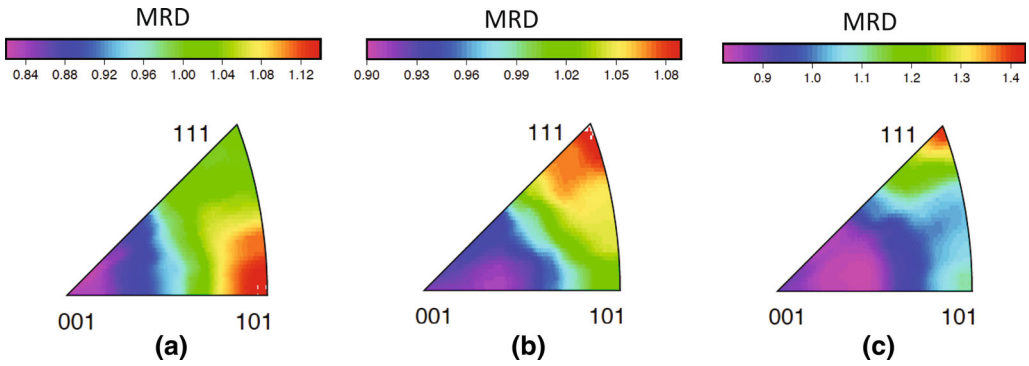

Fig. 5—The distribution of grain boundary planes independent of misorientation for the ferritic microstructures formed through different thermomechanical routes: (*a*) route B, (*b*) route C, and (*c*) route D. MRD is multiples of a random distribution. (b) and (c) are printed with permission from Refs. [5] and [6], respectively.

shown elsewhere that in the case of strong texture with a single misorientation axis, the highest and lowest misorientation angles are statistically favored and the distribution is constant between these limits, consistent with the distribution in Figure 3(c).[14]

The thermomechanical processing routes also altered significantly the grain boundary plane distribution ignoring misorientation angle (Figure 5). For the ferritic microstructure transformed from the recrystallized austenite, the distribution revealed a slight anisotropy with a peak at the position of (101) having a value of 1.14 multiples of a random distribution. The minimum was positioned at (100) having 0.82 MRD. The (111) orientation had ~1 MRD (Figure 5(a)). The maxima at the (101) orientation would be expected for the ferritic microstructure, as the (101) plane has the highest packing factor in the body-centered cubic structure and has a minimum energy.[15] The grain boundary

plane anisotropy slightly decreased for the ferrite transformed from the pancaked austenite (*i.e.*, route C), though the maximum appeared at (111) planes with 1.09 MRD (Figure 5(b)). The static recrystallization of ferrite significantly enhanced the (111) population to 1.36 MRD (*i.e.*, route D, Figure 5(c)). The change in the grain boundary plane distribution is consistent with the texture development of these ferritic microstructures (Figure 4). It appeared that the presence of (111) plane population enhances with an increase in the γ-fiber texture (Figure 4). In other words, the overall texture not only changes the grain boundary misorientation distribution (Figure 3), but also influences the plane/s on which the boundaries are terminated (Figure 5).

The annealing twin boundary, $\Sigma 3 = 60$ deg/[111], was present in all ferritic microstructures, having a population of less than 3 pct. Figure 6 shows the distribution of grain boundary planes for boundaries with a 60 deg/[111] misorientation in the ferritic microstructures formed by different thermomechanical routes. The distribution is plotted as a stereographic projection in the bi-crystal reference frame, where the position of [001] crystal axis is perpendicular to the page and the [100] direction is positioned horizontally in the plane of the paper toward the right. The distribution of grain boundary planes for 60 deg/[111] was qualitatively similar for all ferritic microstructures formed by different thermomechanical routes. The largest grain boundary populations are found along the zone of tilt boundaries (*i.e.*, the great circle perpendicular to the [111] axis), having the maxima at the $(\bar{2}11)$, $(\bar{1}\bar{1}2)$, $(1\bar{2}1)$ symmetric tilt boundary positions (Figures 6(a) through (c)). For the $\Sigma 3$ misorientation, the $\{112\}//\{112\}$ symmetric tilt grain boundaries are coherent twin boundaries for bcc materials.[16] The minimum population appeared at the position of (111)//(111) pure twist boundary, which is the coherent twin boundary for face-centered cubic (fcc) materials.[17] This distribution is inversely correlated to the grain boundary energy distribution measured for a ferritic structure with a similar composition.[5] Indeed, the positions of the $(\bar{2}11)$, $(\bar{1}\bar{1}2)$, $(1\bar{2}1)$ symmetric tilt boundaries and (111) twist appeared as minimum and maximum energy, respectively (Figure 6d). The thermomechanical processing routes did not change the shape of the distribution, though the value of the maxima decreased with an increase in the γ-fiber texture, *i.e.*, from 45 MRD for the ferrite transformed from the recrystallized austenite

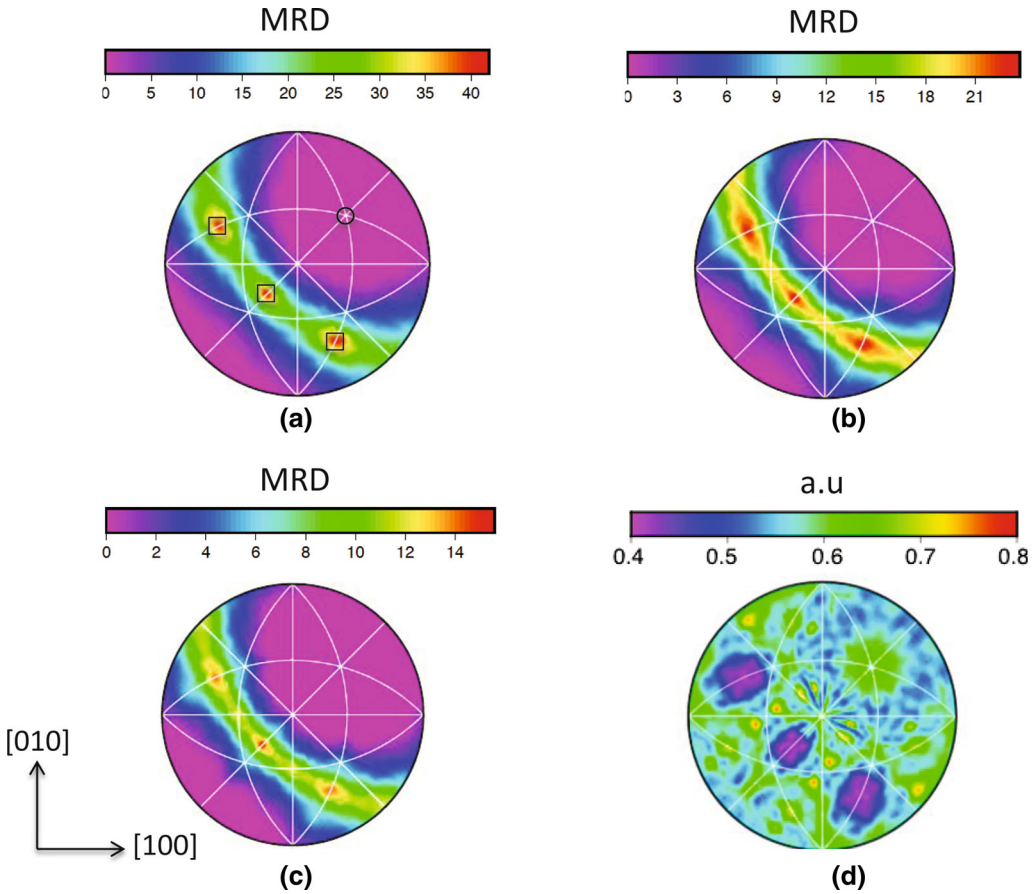

Fig. 6—(*a–c*) the distribution of grain boundary planes at a fixed misorientation of 60 deg/[111] for the ferritic microstructures formed through different thermomechanical routes, plotted in stereographic projection along [001]: (a) route B, (b) route C, and (c) route D. (*d*) The distribution of grain boundary energy at 60 deg/[111] for the ferritic microstructure. Circle and square in "a" represent the position of (111)//(111) twist and (112)//(112) symmetric tilt boundaries, respectively. MRD and a.u are multiples of a random distribution and arbitrary unit, respectively. (b, d) and (c) are printed with permission from Refs. [5] and [6], respectively.

(route B) to ~16 MRD for the ferrite at the statically recrystallized condition (route D, Figure 6). This shows that the texture alters the population of grain boundaries, though it does not change the shape of the grain boundary plane distribution at this misorientation.

B. *The Role of the Phase Transformation Path on the Grain Boundary Character Distribution*

The water quenching of recrystallized austenite led to the formation of a fully martensitic structure (route A) consisting of very fine lath with a high dislocation density (Figure 2(a)). Each prior austenite grain is theoretically transformed into maximum of 12 or 24 distinct orientations/variants, depending on the orientation relationship between the parent austenite and martensite. As the carbon content of the steel used in the current study is very low (*i.e.*, 0.04 wt pct C, Table I), it can be assumed that the OR is close to K–S. As a result, a given austenite grain can be transformed into as many as 24 variants, as listed in Table III. These crystallographic variants can be classified into four distinct families, where the laths in a given crystallographic family have a similar austenite habit plane (*e.g.*, V1 through V6, Table III). The impingement of these variants results in 23 misorientation angle pairs. Due to the crystal symmetry, the intervariant boundaries can be reduced to only 16 distinct misorientations. As a result, the misorientation angle distribution of martensite (Figure 7(a)) was significantly different from that of ferrite transformed from the recrystallized austenite (Figure 3(a)). The misorientation angle distribution of martensite revealed two main peaks at misorientation angle ranges of ~10 to 15 and ~50 to 60 deg. This is consistent with what is expected from the theoretical intervariant misorientation angles associated with the K–S OR (Table III). A low misorientation population also appeared in the range of 20 to 40 deg. This most likely originated from the impingement of variants at the prior austenite grain boundaries. As these variants formed from two distinct adjacent prior austenite grains, the resultant misorientations do not necessarily match the theoretical misorientations expected from the K–S OR.

Figure 7(b) shows the intervariant boundary fraction of martensite, which is significantly different from the ferrite formed through route B. The intervariant boundaries in martensite mostly belonged to those from the same crystallographic family. A second highest population of intervariant boundaries was related to the V1–V2 = 60 deg/[11-1], which has the twin relationship (*i.e.*, Σ3, Figure 7(b)). It was demonstrated that the twin-related laths contain shear components with precisely opposite shape strains. This configuration results in the cancelation of the strains and therefore promotes the shear transformation.[18] It was also shown that the twin-related intervariant boundaries exhibit similar habit planes.[19] The intervariant plane character distribution for the twin-related laths (*i.e.*, Σ3) displayed multiple peaks mainly centered on the zone axis of the tilt boundaries (Figure 8(a). Similar to the ferritic microstructures, a minimum was centered at the (111) twist boundary position. However, the twin-related boundaries for the lath martensite were mostly terminated on {110} planes (*i.e.*, {110}//{110} symmetric tilt boundaries), rather than {112} symmetric tilt boundaries as observed for ferritic structures (Figures 6(a)

Table III. Possible Twenty-Four Variants Generated Through Phase Transformation Having K–S Orientation Relationship

Variant	Plane Parallel	Direction Parallel	Rotation Angle/Axis from V1
V1	(111)γ//(011)α	[-101]γ//[-1-11]α	—
V2		[-101]γ//[-11-1]α	60 deg/[1–11]
V3		[01-1]γ//[-1-11]α	60 deg/[0-1-1]
V4		[01-1]γ//[-11-1]α	10.53 deg/[011]
V5		[1–10]γ//[-1-11]α	60 deg/[011]
V6		[1–10]γ//[-11-1]α	49.47 deg/[0-1-1]
V7	(1-11)γ//(011)α	[10-1]γ//[-1-11]α	49.7 deg/[-1-11]
V8		[10-1]γ//[-11-1]α	10.53 deg/[1–11]
V9		[-1-10]γ//[-1-11]α	50.51 deg/[-16 5 -20]
V10		[-1-10]γ//[-11-1]α	50.51 deg/[-21 -13 14]
V11		[011]γ//[-1-11]α	14.88 deg/[16 6 1]
V12		[011]γ//[-11-1]α	57.21 deg/[-10 17 20]
V13	(-111)γ//(011)α	[0-11]γ//[-1-11]α	14.88 deg/[6–16]
V14		[0-11]γ//[-11-1]α	50.51 deg/[-14 13 -21]
V15		[-10-1]γ//[-1-11]α	57.21 deg/[-21 -7 18]
V16		[-10-1]γ//[-11-1]α	20.61 deg/[20]
V17		[110]γ//[-1-11]α	51.73 deg/[-20 11 -20]
V18		[110]γ//[-11-1]α	47.11 deg/[-22 -9 19]
V19	(11-1)γ//(011)α	[-110]γ//[-11-1]α	50.51 deg/[-5 20 16]
V20		[10-1]γ//[-11-1]α	57.21/[10 20 -17]
V21		[0-1-1]γ//[-1-11]α	20.61/[29 0 -9]
V22		[0-1-1]γ//[-11-1]α	47.11 deg/[-9 19 22]
V23		[101]γ//[-1-11]α	57.21 deg/[-7 -18 -21]
V24		[101]γ//[-11-1]α	21.06 deg/[20 -9 0]

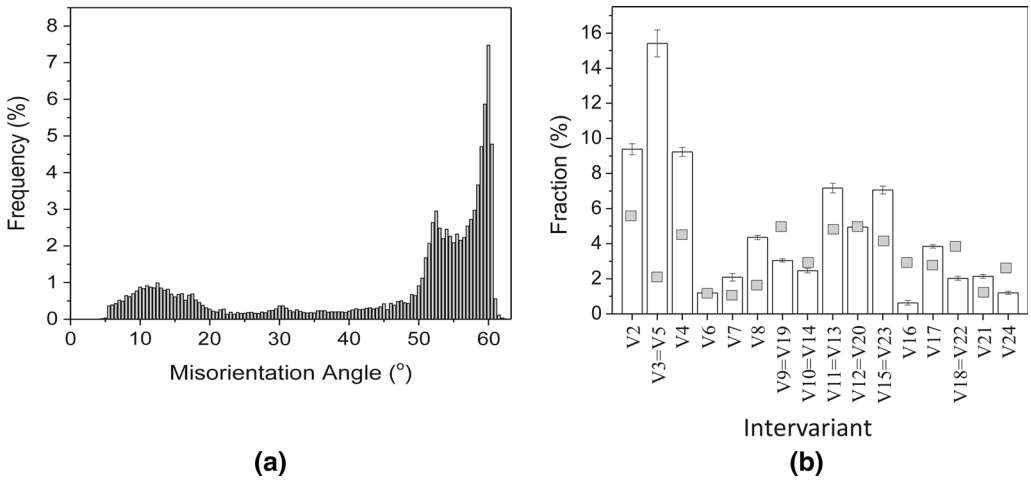

Fig. 7—(*a*) misorientation angle distribution of the martensitic microstructure. (*b*) the fraction of total population of interfaces that belong to K–S OR, comparing intervariant interfaces between V1 and V_i (I = 2–24) for the martensite (*i.e.*, column) and polygonal ferrite (*i.e.*, square). The highest fraction of interfaces belongs to the same crystallographic packet (V1–V5) from Ref. [3]. Because of symmetry, there are only 16 independent intervariant interfaces and "=" sign shows two equivalent intervariant interfaces. Printed with permission from Ref. [3].

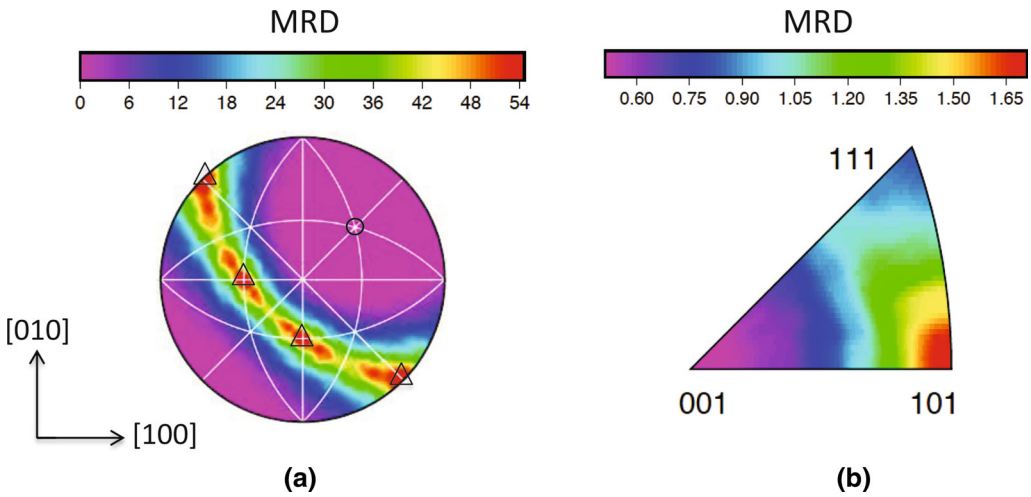

Fig. 8—(*a*) The distribution of grain boundary planes at a fixed misorientation of 60 deg/[111] (a) and independent of misorientation (*b*) for the martensitic microstructure, plotted in stereographic projection along [001]. Circle and triangle in "a" represent the position of (111)//(111) twist and (110)//(110) symmetric tilt boundaries, respectively. MRD is multiples of a random distribution. Printed with permission from Ref. [3].

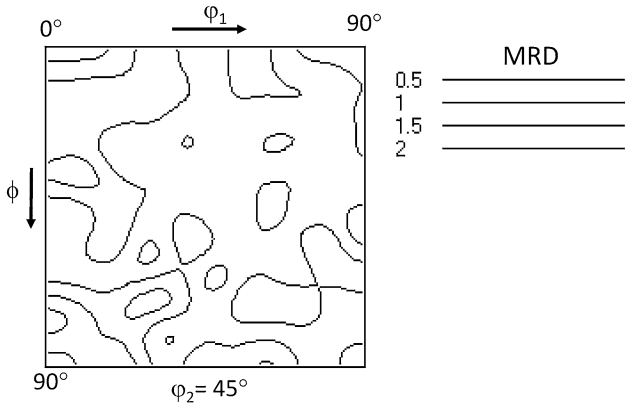

Fig. 9—Orientation distribution function of the martensitic microstructure. MRD is multiples of a random distribution.

through (c)). This is mostly consistent with the reported habit planes measured by TEM for the lath martensitic microstructures by others (*e.g.*, (110),[18,19] near (110),[20] (541),[21] (321)[22]), which mostly lay on the zone axis of tilt boundaries.

Considering the crystallographic constraint associated with the shear transformation (*i.e.*, matching the close-packed planes of martensite and adjacent parent austenite, {111}γ//{110}α), any two crystallographic variants are, most likely, impinged on {110} planes during the martensitic phase transformation. This resulted in a significant anisotropy in the grain boundary plane distribution of martensite, where most boundaries were terminated at {110} planes irrespective of the misorientation (Figure 8(b)). The maximum was ~1.67 MRD, which is 67 pct higher than expected for the random distribution. This suggests that the martensitic transformation causes the boundaries to terminate at

(110) planes, which are coincident with the low-energy plane in bcc materials. Interestingly, the texture of martensite was qualitatively similar to the ferrite formed through route B (Figures 4(a) and 9). Therefore, the change in the misorientation angle distribution of martensite compared with ferrite mainly results from the shear transformation rather than the texture (Figures 3(a) and 7(a)).

III. GENERAL DISCUSSION

Recent advances in both the acquisition and analysis of grain boundary crystallography data have made it possible to measure the grain boundary plane distribution in a wide range of materials with different crystal structures.[5,17,23–26] These measurements display a significant anisotropy in the grain boundary plane distribution for most materials. The crystal structure mostly dictates the preferred planes, which match well with the identical low-energy, low-index planes. For instance, {110} planes are preferred in the case of ferritic steel with the bcc crystal structure (Figure 5(a)), having low energy due to its close-packed configuration.[15] There is also a strong inverse correlation between the grain boundary population and energy,[5,17,23,24] where low-energy boundaries are observed more frequently in the distribution than high-energy boundaries (Figure 6). The theory for the origin of this distribution requires some grain growth, during which high-energy boundaries are preferentially eliminated.[27] This mechanism will obviously not be relevant to microstructures formed by transformation with little grain growth.

The current results illustrate what can happen when the importance of the grain boundary energy is overwhelmed by the influence of the phase transformation mechanism and the exact processing route. In the fully ferritic microstructures, the processing route alters the orientation texture, which ultimately influences the distribution of grain boundary misorientations, the preferred habit planes, and the anisotropy of the grain boundary character distribution. Here, it is clearly demonstrated that the population of (111) planes increases with an increase in the γ-fiber texture (Figures 3 through 5). However, the texture resulting from different thermomechanical routes did not alter the shape of the distribution at specific misorientations. For instance, the grain boundary plane distribution for the $\Sigma 3$ boundary in ferrite reveals strong peaks at the positions of the $(\bar{2}11)$, $(\bar{1}\bar{1}2)$, $(1\bar{2}1)$ symmetric tilt boundaries, which appear to have a minimum energy in bcc crystal structure (Figure 6). While the maxima are in the same positions, the relative areas differ (Figure 6). The relative areas of the tilt boundaries decrease with an increase in the γ-fiber texture.

The most significant changes are observed when the mechanism of phase transformation alters from diffusional (*i.e.*, ferrite) toward shear/diffusionless (*i.e.*, martensite) transformation. A change in the phase transformation path reveals remarkable changes in both the misorientation angle distribution (Figure 7(a)) and the characteristics of preferred habit planes for a given misorientation (Figure 8(a)). The misorientation angle distribution of the martensitic structure qualitatively differs from polygonal ferrite microstructures formed through different thermomechanical routes (Figures 3(a) and 7(a)). In general, it has a bimodal distribution, which closely matches the theoretical intervariant misorientation angle ranges expected from the K–S orientation relationship (Table III). Interestingly, the interface plane orientation distribution of the $\Sigma 3$ boundary for the martensitic microstructure shows maxima at {110} symmetric tilt planes, rather than the {112} as observed for ferritic microstructures (Figures 6 and 8(a)). This is consistent with the crystallographic constraints associated with the martensitic transformation rather than low-energy configuration as {110} has a relatively higher energy compared with {112} orientation for this grain boundary (Figure 6(d)). A similar observation was reported for the grain boundary character distribution of martensite in a Ti-6Al-4V alloy.[4]

The findings presented here show that processing can be used to alter the grain boundary character distribution. Instead of distributions controlled purely by the grain boundary energy anisotropy, that result from normal grain growth, appropriate processing routes can be used to engineer the grain boundary character distribution. This important finding provides a path for the development of novel processing routes to engineer sustainable materials at the mesoscale level through controlling the population of different grain boundary types. This will require a new level of fundamental understanding of grain boundary network formation through different processing routes and transformation paths, and its effect on mechanical and other material properties.

IV. CONCLUSION

The properties of interfaces depend not only on the lattice misorientation, but also on the interface plane orientation. Extensive studies of grain boundaries led to the conclusion that in systems evolving by normal grain growth, the relative areas of different grain boundary planes are inversely correlated to their relative energies.[17,23–26] In other words, low-energy grain boundary planes make up a larger part of the population than the higher energy grain boundary planes. The current results, however, revealed that the interface plane orientation distributions in transformed microstructures do not necessarily follow the relative energy. Instead, the interface plane orientation distributions in these microstructures depend more on the mechanism of formation. The thermomechanical processing route significantly influenced the extent of anisotropy in the grain boundary character distribution through altering the overall texture of phase-transformed products (*e.g.*, ferrite) and/or the phase transformation path (*i.e.*, ferrite *vs* martensite). For example, the enhancement of γ-fiber texture in the ferritic microstructure through thermomechanical processing increased the population of low-angle boundaries and promoted grain boundaries terminated by (111) planes. However, it did not alter the

habit plane characteristics in a specific misorientation. For the Σ3 (60 deg/[111]) misorientation in the fully ferritic structures produced through different routes, {112} symmetric tilt boundaries had the highest population and lowest energy. On the other hand, the phase transformation path (*i.e.*, ferrite *vs* martensite) remarkably changed the distribution of grain boundary normals for a given misorientation. In the martensitic steel, for the Σ3 boundary, {110} symmetric tilt boundaries were the most common. This results from the crystallographic constraints associated with the shear transformation (*i.e.*, martensite) rather than the low-energy interface that dominates in the diffusional phase transformation (*i.e.*, ferrite). The sensitivity of the grain boundary type to the phase transformation path can potentially lead to a new thermomechanical processing route to engineer the grain boundary network for specific applications.

ACKNOWLEDGMENTS

The work at Deakin University was supported through grants provided by Australian Research Council. This work was carried out with the support of the Deakin Advanced Characterization Facility. G.S.R. acknowledges support from the ONR-MURI program (Grant No. N00014-11-0678) and the use of the Materials Characterization Facility at Carnegie Mellon University supported by Grant MCF-677785.

REFERENCES

1. T. Watanabe: *Trans. Jpn. Inst. Metals*, 1986, vol. 27, pp. 73–82.
2. V. Randle: *Acta Metall.*, 1999, vol. 47, pp. 4187–96.
3. H. Beladi, G.S. Rohrer, A.D. Rollett, V. Tari, and P.D. Hodgson: *Acta Mater.*, 2014, vol. 63, pp. 86–98.
4. H. Beladi, Q. Chao, and G.S. Rohrer: *Acta Mater.*, 2014, vol. 80, pp. 478–89.
5. H. Beladi and G.S. Rohrer: *Acta Mater.*, 2013, vol. 61, pp. 1404–12.
6. H. Beladi and G.S. Rohrer: *Metall. Mater. Trans. A*, 2013, vol. 44, pp. 115–24.
7. D.Q. Bai, S. Yue, W.P. Sun, and J.J. Jonas: *Metall. Mater. Trans. A*, 1993, vol. 24, pp. 2151–59.
8. K.J. Irvine: J of Iron Institute, 1967, pp. 161-67.
9. G.S. Rohrer, D.M. Saylor, B. El Dasher, B.L. Adams, A.D. Rollett, and P. Wynblatt: *Zeitschrift Für Metallkde.*, 2004, vol. 95, pp. 1–18.
10. R.K. Ray and J.J. Jonas: *Inter. Mater. Rev.*, 1990, vol. 35, pp. 1–36.
11. G.J. Baczynski, J.J. Jonas, and L.E. Collins: *Metall. Mater. Trans. A*, 1999, vol. 30, pp. 3045–54.
12. L Kestens and JJ Jonas: in *ASM Handbook*, SL Semiatin, ed., ASM International, Materials Park, 2005, vol. 14A, pp. 685–700.
13. H.K.D.H. Bhedeshia: *Bainite in Steels*, 2nd ed., IOM Communications Ltd., London, 2001.
14. R.E. Garcia and M.D. Vaudin: *Acta Mater.*, 2007, vol. 55, pp. 5728–35.
15. B. Gale, R.A. Hunt, and M. McLean: *Philos. Magn.*, 1972, vol. 25, pp. 947–60.
16. J.P. Hirth and L. Lothe: *Theory of Dislocations*, 2nd ed., Krieger Publishing Company, Florida, 1982, pp. 274–366.
17. H. Beladi, N.T. Nuhfer, and G.S. Rohrer: *Acta Mater.*, 2014, vol. 70, pp. 281–89.
18. P.M. Kelly, A. Jostsons, and R.G. Blake: *Acta Mater.*, 1990, vol. 38 (1990), pp. 1075–81.
19. P.M. Kelly: *Acta Metall.*, 1965, vol. 13, pp. 635–46.
20. F. Duflos and B. Cantor: *Acta Metall.*, 1982, vol. 30, pp. 323–42.
21. A. Van Gent, F.C. Van Doorn, and E.J. Mittermeijer: *Metall. Trans. A*, 1985, vol. 16, pp. 1371–84.
22. J.M. Chilton, C.J. Barton, and G.R. Speich: *J. Iron Steel Inst.*, 1970, vol. 208, p. 184.
23. D.M. Saylor, A. Morawiec, and G.S. Rohrer: *Acta Mater.*, 2003, vol. 51, pp. 3675–86.
24. D.M. Saylor, B.S. El-Dasher, T. Sano, and G.S. Rohrer: *J Amer. Cer. Soc.*, 2004, vol. 87, pp. 670–76.
25. J. Li, S.J. Dillon, and G.S. Rohrer: *Acta Mater.*, 2009, vol. 57, pp. 4304–11.
26. D.M. Saylor, B.S. El-Dasher, A.D. Rollett, and G.S. Rohrer: *Acta Mater.*, 2004, vol. 52, pp. 3649–55.
27. S.J. Dillon and G.S. Rohrer: *Acta Mater.*, 2009, vol. 57, pp. 1–7.